Giant Quantum Oscillations in High-Purity Bismuth: Search for Hole-Fermi-Surface Anomalies*

Victor E. Henrich
Lincoln Laboratory, Massachusetts Institute of Technology, Lexington, Massachusetts 02173
(Received 27 June 1972)

The Fermi surface of holes and electrons in bismuth has been investigated by means of giant quantum oscillations in the ultrasonic attenuation in an attempt to explain the anomalies in the hole Fermi surface reported by Giura *et al*. The properties of giant quantum oscillations are reviewed, with emphasis on the effects of finite-carrier relaxation time on nonextremal orbits. Experiments were performed on very high-quality single crystals ($\tau \sim 6$ nsec), and all sheets of the Fermi surface were studied. The complete disappearance of oscillations previously observed was not seen. Except for one orientation in which nonextremal areas were observed, all oscillations were due to extremal orbits (as were those reported by Giura *et al.*). Thus, effects due to a nonextremal orbit tangent to a saddle point on the Fermi surface, as suggested by Giura *et al.*, could not occur. It is suggested that the anomalies may have been caused by crystal misorientation.

I. INTRODUCTION

The Fermi surface of bismuth has been studied so extensively in the past that one wonders if there is any information yet to be obtained about it. Three years ago, however, Giura *et al.*[1] reported some anomalies in the attenuation of ultrasound in bismuth crystals. They found that giant quantum oscillations in the ultrasonic attenuation disappeared for certain orientations other than those predicted by theory.[2] Since these oscillations are theoretically capable of measuring *nonextremal* Fermi-surface orbits in the region of their measurements, they suggested that the disappearance of the oscillations might be explained by the breakdown of Landau-level quantization when the plane of a nonextremal hole orbit was tangent to a saddle point on the hole Fermi surface. Presumably the planes of the extremal orbits seen in most experiments would never be tangent to the Fermi surface, and such a quantization breakdown could not occur.

Since the existence of such a saddle point would be most interesting, we undertook a careful study of the giant quantum oscillations in the attenuation of 185-MHz longitudinal ultrasound in very high-quality bismuth single crystals at 1.5 °K. Nonextremal areas were observed in only one orientation, and that was 90 ° away from the region of the proposed saddle point. In the vicinity of the saddle point, neither disappearance of signal nor nonextremal areas were observed, and examination of the previous data shows that only extremal areas were seen there, also. The possibility that nonextremal areas tangent to a saddle point are causing the anomalies is thus ruled out. Some suggestions as to the possible cause of signal disappearance in terms of sample misorientation are presented.

In Sec. II, the theory of giant quantum oscillations is reviewed, with particular attention paid to the region where nonextremal orbits might be seen. The importance of finite-carrier relaxation time is also considered. In Sec. III, sample preparation, experimental procedure, and data analysis are described. In Sec. IV, the observation of oscillations due to nonextremal areas and the agreement between theoretical and experimental line shape of these oscillations is reported. The unambiguous observation of these orbits is central to the identification of oscillations seen in an ultrasonic-attenuation experiment. In Sec. V, the results of extensive measurements in the regions where disappearance of oscillations was previously reported are described.

II. REVIEW OF GIANT-QUANTUM-OSCILLATION THEORY

A. Limit of $\tau = \infty$, $T = 0$ °K

Giant quantum oscillations in the attenuation of a beam of ultrasound were first predicted by Gurevich, Skobov, and Frisov.[2] These oscillations arise when conduction electrons (or holes) absorb energy from the acoustic phonon beam in the presence of a magnetic field of sufficient strength that the Landau-level separation is larger than the phonon energy. The electrons must then remain on the same Landau level after the absorption ($\Delta n = 0$), putting severe restrictions on the allowed initial states of electrons that can participate. In the limit of large carrier relaxation time τ the resulting attenuation exhibits large, spikelike peaks which are easily distinguishable from density-of-states (de Haas–van Alphen-type) oscillations (for example, see Fig. 8).

Both energy and the component of momentum

(or wave vector) along the magnetic field direction must be conserved in this process. Assuming a parabolic band and no broadening of the Landau levels ($\tau = \infty$, $T = 0\,^\circ$K), conservation of energy and momentum gives

$$\frac{\hbar^2 k_H^2}{2m_H} + \hbar\omega = \frac{\hbar^2 (k_H + q_H)^2}{2m_H} , \tag{1}$$

where $\hbar k_H$ is the component of electron momentum along the magnetic field $\vec{H}$, m_H is the electron effective mass along $\vec{H}$, ω is the frequency of the sound wave, and $\hbar q_H$ is the component of phonon momentum along $\vec{H}$.

If the sound wave vector is inclined an angle θ away from $\vec{H}$, the phonon momentum along $\vec{H}$ is

$$\hbar q_H = \hbar q \cos\theta , \tag{2}$$

so that Eq. (1) becomes, after cancelling two terms

$$\frac{\hbar k_H}{m_H} = \frac{\omega}{q\cos\theta} - \frac{\hbar q \cos\theta}{2m_H} . \tag{3}$$

Since ω/q is the phase velocity of the sound wave v_s, and $\hbar k_H/m_H$ is the electron velocity in the direction of $\vec{H}$ averaged over the orbit $\langle v_H \rangle$, Eq. (3) can be written

$$\langle v_H \rangle = \frac{v_s}{\cos\theta} - \frac{\hbar q \cos\theta}{2m_H} . \tag{4}$$

In most cases, the last term in the right is small, and in the interesting region of $\theta \approx 90\,^\circ$, it vanishes. If we neglect it, we see that the electrons that are allowed to absorb a phonon are just those that are drifting in phase with the sound wave. In bismuth, as in most metals and semimetals, the electron velocity at the Fermi level in zero magnetic field v_F is two or three orders of magnitude larger than v_s. Thus in Eq. (4), $\langle v_H \rangle$ will be much smaller than v_F unless θ is very near $90\,^\circ$; that is, unless the sound wave is nearly perpendicular to the magnetic field.

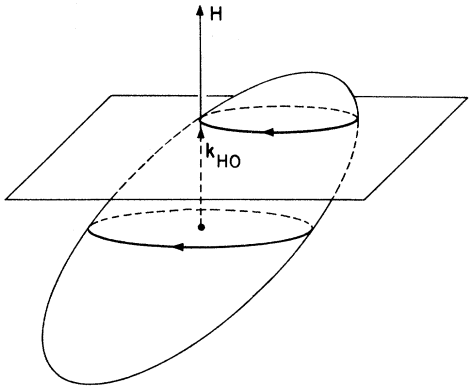

FIG. 1. Extremal and nonextremal Fermi-surface orbits.

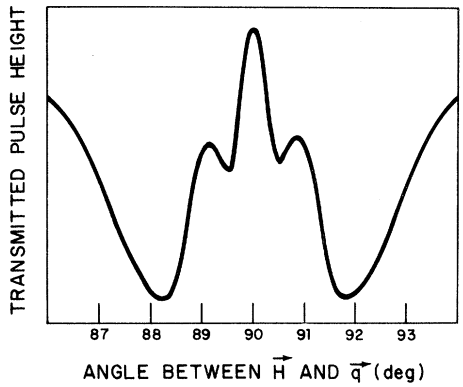

FIG. 2. Experimental transmitted ultrasonic pulse height vs relative orientation of $\vec{H}$ and $\vec{q}$ near $\vec{H} \perp \vec{c}$: the "tilt effect."

The behavior near $\theta = 90\,^\circ$ can better be seen in terms of the electron wave vector (or momentum). From Eq. (3), the $\vec{H}$ component of electron wave vector necessary for phonon absorption is

$$k_{H0} = \frac{v_s}{\cos\theta} \frac{m_H}{\hbar} , \tag{5}$$

where we have dropped the last term on the right-hand side since it goes to zero when $\theta = 90\,^\circ$. Unless θ is nearly $90\,^\circ$, k_{H0} will be essentially zero on the scale of the zero-field Fermi-level value, k_{HF}. Giant quantum oscillations then occur when a Landau level passes the Fermi level at $k_H \approx 0$. These oscillations have the usual de Haas–van Alphen periods and measure the *extremal* cross sectional areas of the Fermi surface (see Fig. 1). Their shape is spikelike, however, unlike density-of-states oscillations. As θ approaches $90\,^\circ$, k_{H0} increases, eventually becoming comparable to k_{HF}. Peaks in the attenuation still occur when a Landau level crosses the Fermi level at k_{H0}, but now this corresponds to an electron orbit whose plane is a distance k_{H0} away from the center of the Fermi surface, as in Fig. 1. This orbit is referred to as *nonextremal*. Since k_{H0} becomes infinite when $\theta = 90\,^\circ$, there will be a range of angles around $90\,^\circ$ where k_{H0} is larger than k_{HF}, and the plane of the "orbit" no longer intersects the Fermi surface. No electrons can then contribute to the attenuation. This gives rise to an increase in the transmitted pulse height at $\theta = 90\,^\circ$, as shown in Fig. 2. This is the tilt effect,[3] and its sharpness allows the relative orientation of $\vec{q}$ and $\vec{H}$ to be determined to about $0.1\,^\circ$. In addition, the quantum oscillations disappear completely whenever $k_{H0} > k_{HF}$.

In bismuth at liquid-helium temperatures, the conditions for giant quantum oscillations are easily met for sound frequencies around 200 MHz if the

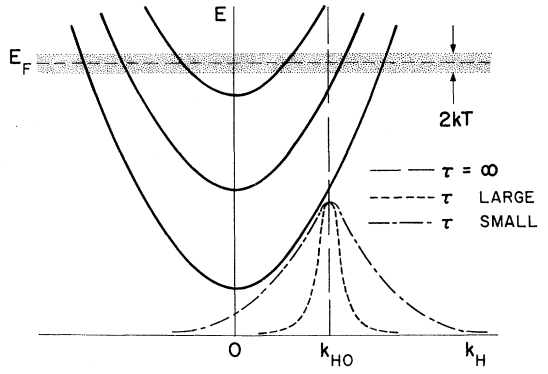

FIG. 3. Effects of finite-carrier relaxation time on giant quantum oscillations; see text for explanation.

magnetic field is greater than several hundred gauss. The measurements we will be describing were done using 185-MHz sound and magnetic fields from 1 to 15 kG. In this region only $\Delta n = 0$ processes are allowed, so all data should be interpretable in terms of giant quantum oscillations.

B. Carrier Relaxation and Finite Temperature

From the above discussion, ultrasonic giant quantum oscillations seem like the ideal way to investigate *all* cross sectional areas of a Fermi surface simply by changing the magnetic field orientation. Unfortunately, the effects of finite carrier relaxation time all but eliminate the nonextremal nature of the oscillations. When finite temperature T and relaxation time τ are included, the theory of Gurevich *et al.*[2] (including the correction pointed out by Svirskii[4]), gives for the ultrasonic attenuation

$$\text{Atten.} \sim \frac{H}{T}\sum_n \int_{-\infty}^{\infty} dk_H \times \left\{ \frac{1}{\tau} \Big/ \left[\frac{1}{\tau^2} + \left(\frac{\hbar k_H q \cos\theta}{m_H} + \frac{hq^2 \cos^2\theta}{2m_H} - \omega \right)^2 \right] \right\} \times \cosh^{-2}\left(\frac{\hbar\omega_c (n+\frac{1}{2}) \pm \frac{1}{2} g\mu_B H + \hbar^2 k_H^2/2m_H - E_F}{2kT} \right), \tag{6}$$

where ω_c is the electron cyclotron frequency. The first term in the integral, a Lorentzian in $k_H - k_{H0}$, expresses the relaxation of the energy and momentum conservation conditions due to finite τ. The last term represents the thermal population of the Landau levels at the Fermi level.

This expression can be interpreted graphically in Fig. 3. The Landau-level spacing shown is characteristic of many orientations in bismuth when the magnetic field is about 10 kG. The thermal smearing of the Fermi surface is represented by the shaded area around E_F; only electrons in this region can contribute to the attenuation due to the availability of both initial and final states. If $\tau = \infty$, the relaxation-time Lorentzian becomes a δ function at $k_H = k_{H0}$. Peaks in the attenuation occur when the intersection of a Landau level and the vertical dashed line (δ function) at k_{H0} lies in the shaded area. The shape of the attenuation peaks would be given solely by the $\cosh^{-2}$ term in Eq. (6). The period of the oscillations (in $1/H$) would give the Fermi-surface area at k_{H0}.

If τ is finite but large, electrons in the momentum region given by the dashed Lorentzian can contribute to the attenuation. This results in further broadening of the attenuation peaks and possible averaging of areas due to several Landau levels. As τ becomes smaller, the distribution of allowed values of k_H broadens until it eventually has a significant contribution at $k_H = 0$. Owing to the high density of states there, additional peaks will occur in the attenuation corresponding to extremal area, de Haas–van Alphen-type oscillations. The simultaneous appearance of these oscillations and the broad giant quantum oscillations can be clearly seen in the experimental curves considered in Sec. IV (see Fig. 6). Since the width of the Lorentzian is proportional to k_{H0}, its amplitude at $k_H = 0$ is independent of k_{H0}, so external oscillations can occur even if $k_{H0} > k_{HF}$, at least within the limits of the Gurevich theory. In the limit of $\tau \to 0$, the Lorentzian is infinitely broad, and all electrons near E_f can contribute. Then only the de Haas–van Alphen-type oscillations remain, and only extremal areas can be measured.

As discussed in Ref. 5, electron relaxation effects are so important in practice that the only clear observation of nonextremal orbits has been in one of our two bismuth samples. Since the relaxation-time Lorentzian has a width which is proportional to k_{H0}, it can be very narrow on the scale of k_{HF} when $k_{H0} \approx 0$, even for small τ. Thus the characteristic spikelike attenuation peaks can be observed even though the orbits contributing are extremal. As θ approaches 90°, however, the Lorentzian broadens so much that the giant quantum oscillations spread out and disappear before nonextremal orbits can be seen. This is a crucial point in the interpretation of Fermi-surface topology from ultrasonic-attenuation data, and we shall return to it again when considering experimental results.

III. EXPERIMENT

A. Sample Preparation

The bismuth samples used in this experiment were single crystals pulled from a 99.9999% pure melt with an oriented seed crystal under a hydrogen atmosphere. Two cubes (1 cm on a side) were

spark cut from these boules, then spark planed at low energy and etched. The faces were oriented to within about 2° of the major crystal axes by Laue diffraction. The exact orientation error was determined from Fermi-surface measurements, as will be described later. After etching, grain boundaries and strain marks, if any, were visible. The two samples used showed no visible gain boundaries on any face. They were further checked by x-ray Laue diffraction from all faces, and no trace of polycrystallinity was seen. One of the samples, to be referred to as sample I, showed strain lines on two of its faces. The other one, sample II, showed only a trace of strain in one corner. Except for one orientation in which sample II yielded nonextremal areas,[5] both samples gave the same periods. Sample II did give somewhat larger and sharper attenuation peaks, however.

Small bars, about $1 \times 1 \times 15$ mm, were cut from areas adjacent to the samples and were used to measure the resistivity ratio between 300 and 4.2 °K. Values between 191 and 236 were obtained, which put a lower limit on the value in the large crystals owing to the effects of surface scattering in the small bars.[6]

From studies of the amplitude and shape of giant quantum oscillations due to nonextremal Fermi-surface trajectories,[5] the electron relaxation time τ in one orientation of sample II was calculated to be about 6 nsec at 1.5 °K, consistent with some of the best values reported in bismuth.[7] Values of τ for other orientations in sample II, and for any orientation in sample I, could not be determined owing to the lack of nonextremal oscillations.

B. Ultrasonic-Attentuation Measurements

The ultrasonic attenuation was measured by the standard pulse-transmission method. A block diagram of the experimental setup when measuring the derivative (with magnetic field) of the transmitted pulse height is shown in Fig. 4. X-cut quartz transducers with a fundamental frequency of 20 MHz were bonded to opposite faces of the sample. For most of the measurements reported here, the transducers were run at 185 MHz, slightly above their ninth harmonic. Pulses of rf (1-μsec long) were generated by an Arenberg PG-650C pulsed oscillator. The transmitted pulses were detected with an R-484/APR-14 radar receiver and a lock-in detector. A General Radio audio wave analyzer was used as a narrow-band filter tuned to the modulation frequency (1100 Hz). The solid-state switch and the gate were used to select only the first transmitted pulse for analysis. The magnetic field was measured with a modified rotating coil gaussmeter and an ac-dc converter. (In some measurements a lock-in detector was substituted for the converter.) Linearity and calibration of the field were checked with an NMR gaussmeter. The resulting X-axis display of magnetic field on the X-Y recorder was accurate to 0.4%. The modulating field was about 5 G peak to peak. When the transmitted pulse height itself was to be measured, the wave analyzer was removed and the pulsed oscillator was triggered from the internal reference of the lock-in detector.

The sample holder used for orienting the crystal at liquid-He temperature permitted rotation about

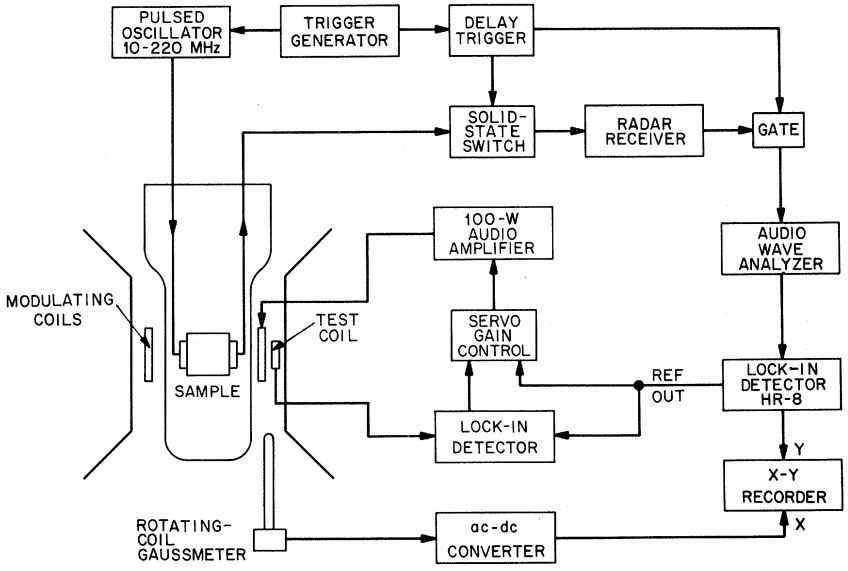

FIG. 4. Experimental setup for measuring ultrasonic attenuation by the transmitted pulse method.

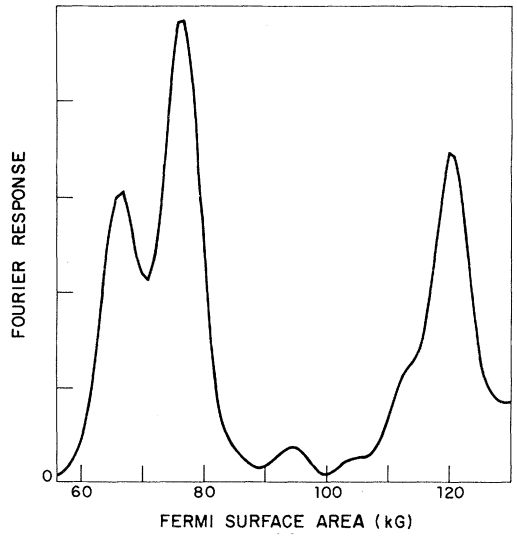

FIG. 5. Fourier spectrum from digital-filter routine; ordinate is linear.

two axes. The sound wave propagated in a horizontal direction and the sample could be rotated a full 360° around this axis. In addition, the sample could be tilted several degrees about the other horizontal axis. The angle most often varied during a run was the direction of the magnetic field relative to the sample holder. The entire magnet (a 12 in. Harvey Wells) could be rotated 360° about a vertical axis, thus rotating the magnetic field in a horizontal plane. Thus only the orientation of $\vec{q}$ relative to the crystal axes was fixed. The two sample holder rotations were repeatable to about 0.2°, while the position of the magnet could be set to 0.1°.

C. Data Analysis

Since the bismuth Fermi surface consists of three electron sheets and one hole sheet, as many as four different oscillations can contribute to the attenuation at once and the resulting wave form can be rather complex (for example, see Fig. 14). In order to accurately determine the frequencies present, Fourier analysis of the data was necessary. The signal-versus-magnetic-field traces were first converted to digital form on a Calma VIP-485/800 digitizing table. Between 600 and 2000 points were taken per curve, depending on the amount of detail present. Subsequent computer processing converted the abscissa to $1/H$ and Fourier analyzed the data. Two types of Fourier analysis were employed. A fast Fourier routine[8] was used initially because of its extreme speed. Regions of interest were then carefully analyzed with a digital-filter routine.[9] This method was chosen over a regular Fourier routine because of its better resolution. An example of the resulting spectra is shown in Fig. 5. If the peaks are well isolated, the accuracy of the frequency determination is about 2%. As two peaks approach one another in frequency, the routine tends to repel the peaks slightly. As they come even closer together, they are attracted before finally merging. In cases where this affected interpretation of the data, a regular slow Fourier analysis was used. This routine was less sensitive to such frequency pulling.

Since the giant quantum oscillations often have a spikelike character, higher harmonics may appear in the Fourier analysis. If the fundamental frequency of one sheet of the Fermi surface is near a harmonic of some other sheet, it is often impossible to clearly identify the higher-frequency oscillation. If there was any question of overlap of this sort, the higher-frequency oscillation was not included. This often leads to a paucity of data for large areas (see Fig. 8), but no spurious areas are considered.

IV. OBSERVATION OF NONEXTREMAL AREAS

The oscillations in the ultrasonic attenuation measured in all configurations of $\vec{q}$, $\vec{H}$, and crystal axes on our samples were found to exhibit all of the properties of giant quantum oscillations seen by other authors.[10] They were of large amplitude and, when the periods were sufficiently long, had a spikelike shape (see Fig. 6). They disappeared when $\vec{H}$ was normal to $\vec{q}$ (see Figs. 10 and 14), and the tilt effect could be clearly observed. But the Fermi-surface areas measured were extremal, even in regions where Eq. (5) predicts a significant departure from extremal. Thus, a search was undertaken of all of the regions where $\vec{q}$ was nearly normal to $\vec{H}$ in an attempt to find evidence for the contribution of electrons with nonextremal orbits. In sample I, no trace of any areas other than extremal was found, even though the signal disappeared when $\vec{H} \perp \vec{q}$. Presumably the electron and hole relaxation times were short enough so that the Lorentzian in Eq. (6) was very broad. In sample II, one orientation was found in which nonextremal areas were clearly present: $\vec{q}$ parallel to the trigonal axis and $\vec{H}$ near the binary axis in the trigonal-binary plane. Excellent agreement was found not only with the measured areas but also with the line shape of the oscillations.[5] (In a second orientation—$\vec{q}$ along the trigonal axis and $\vec{H}$ near the bisectrix axis in the trigonal-bisectrix plane—significant departure from extremal areas was seen in sample II, but, owing to the simultaneous presence of several sheets with similar areas, nonextremal orbits could not be uniquely identified.)

This observation of nonextremal areas has been

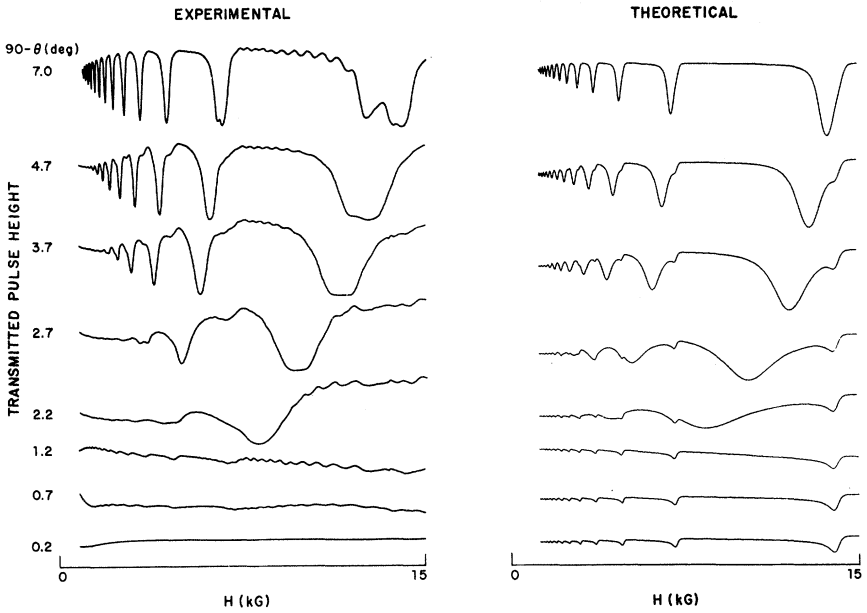

FIG. 6. Experimental and theoretical transmitted pulse height vs magnetic field for sample II. θ is the angle between $\vec{H}$ and $\vec{q}$. $\vec{q}$ is parallel to the trigonal axis and $\vec{H}$ is in the trigonal-binary plane. The theoretical curves were calculated using $\omega\tau = 7$.

reported previously,[5] and we shall only summarize the results here. Figure 6 shows the experimental transmitted pulse-height–versus–magnetic-field data in the vicinity of $\vec{H} \perp \vec{q}$, along with the corresponding curves predicted from the theory of Gurevich *et al.*[2] outlined above. The high-frequency oscillations seen in the data arise from large area hole and electron sheets and were not included in the theory. Also, the spin splitting observed at 7° was neglected. The simultaneous presence of both nonextremal giant oscillations and extremal de Haas–van Alphen-type oscillations, as discussed in Sec. II, can be seen. The fact that the observed disappearance of the de Haas–van Alphen-type signal when $\vec{H} \perp \vec{q}$ is not predicted by the expressions of Gurevich *et al.* represents a weakness in the theory; it will be considered in a future publication.

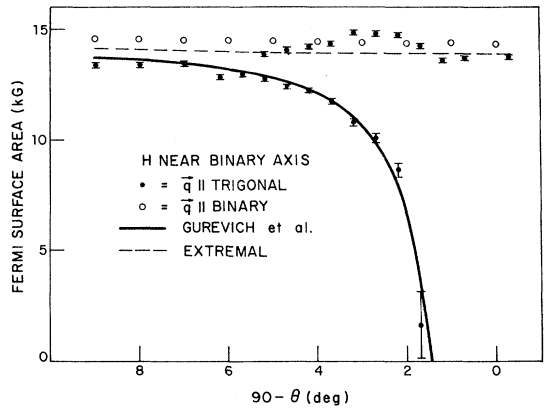

FIG. 7. Fermi-surface areas from data in Fig. 8. With $\vec{q} \parallel$ trigonal axis, θ is the angle between $\vec{H}$ and $\vec{q}$. With $\vec{q} \parallel$ binary axis, $90° - \theta$ is the angle between $\vec{H}$ and $\vec{q}$.

The areas determined from these data, along with areas measured with $\vec{H}$ in the same orientation but with $\vec{q}$ along the binary axis ($\vec{q}$ parallel to $\vec{H}$), are shown in Fig. 7. From the line shape of the oscillations, the electron relaxation time in the binary direction in sample II was determined to be about 6 nsec, consistent with some of the best values reported in bismuth.[7]

We believe that these measurements represent the first unambiguous observation of nonextremal Fermi-surface orbits by giant quantum oscillations reported in any material. They are central to the interpretation of giant-quantum-oscillation data for two reasons. First, they show that the existence of the tilt effect, the disappearance of oscillations when $\vec{H} \perp \vec{q}$ and the large, spikelike attenuation peaks characteristic of giant quantum oscillations do not automatically imply that areas measured when $\vec{H}$ is nearly normal to $\vec{q}$ will be nonextremal; the relaxation time can still be sufficiently short that the nonextremal contribution to the attenuation is too broad and weak to be observable. Second, the agreement of both area and line shape of the nonextremal oscillations make it possible to clearly distinguish them from extremal oscillations if they are present at all. We shall invoke these properties when interpreting ultrasonic-attenuation data below.

V. EXPERIMENTAL FERMI-SURFACE AREAS

A. Survey

With the exceptions mentioned in Sec. IV, all areas observed in our experiments were extremal.

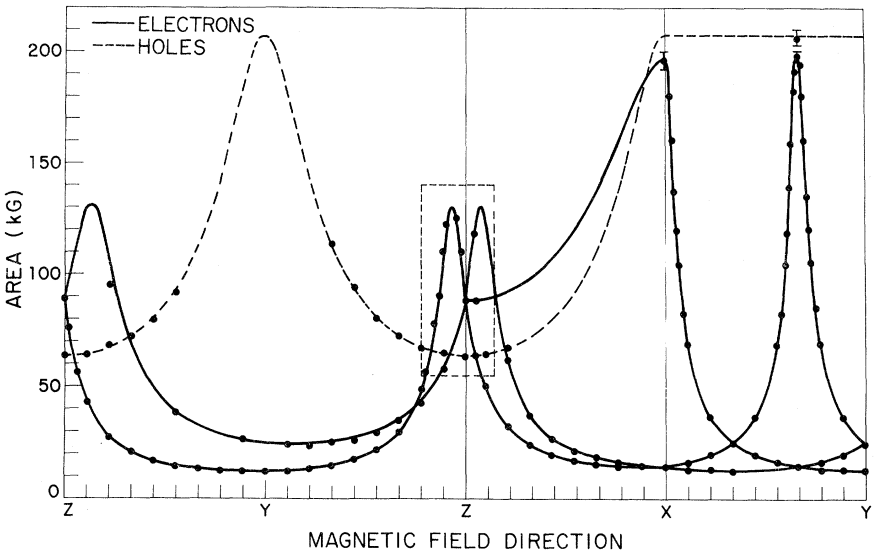

FIG. 8. Bismuth Fermi-surface areas measured in all configurations on both samples. Solid and dashed lines are predicted extremal areas using the masses of Sakai *et al.* (Ref. 11).

Measurements were made on both samples using all configurations of $\vec{H}$, $\vec{q}$ and the three major crystal axes, and the resulting Fermi-surface areas are summarized in Fig. 8. The areas measured on both samples agreed within the experimental error of about 2%. Most branches were measured in more than one configuration, i.e., for a particular orientation of $\vec{H}$, $\vec{q}$ could be along any of the three crystal axes. Not all branches can be observed in all configurations, owing to the varying strength of the signals from the different sheets, but when they could be seen in more than one orientation, the areas agreed. As mentioned previously, the existence of harmonics of the strong, low-frequency oscillations tended to obscure the generally weaker high-frequency ones, so little data are available on several of the large-area branches. If there was any ambiguity in identification of a Fourier component, it was not included. In addition to the bulk of the measurements made at 185 MHz and 1.5 °K, some data were taken at 4.2 °K and/or 20 or 100 MHz. All areas agreed within experimental error.

The solid and dashed lines represent the extremal Fermi-surface areas predicted using the effective masses measured by Sakai *et al.*,[11] except that the value of α_1 was reduced by 5% to fit the electron data near the trigonal axis where the bulk of our measurements were made. It should be stressed that it was not the purpose of this experiment to accurately determine the effective masses, and we are not implying a 5% error in Sakai's value. It is quite possible that smaller adjustments of all four electron masses could have done as well, but attempts at this were not made due to the complexity of the Fermi surface. The exact values of α are not important here, anyway.

The dashed rectangle in Fig. 8 indicates the region in which Giura *et al.*[1] reported the disappearance of oscillations. In both cases, the disappearance occurred when $\vec{H}$ was within a few degrees of the trigonal axis, but in one configuation $\vec{q}$ was along the binary axis while in the other $\vec{q}$ was along the bisectrix axis. We shall consider the two configurations separately since the conclusions drawn about them are slightly different.

B. Binary-Trigonal Plane

With $\vec{q}$ along the binary axis and $\vec{H}$ in the trigonal-binary plane, Giura *et al.* saw the disappearance of oscillations when $\vec{H}$ was 3° or 4° either side of the c axis (see Figs. 5 and 7 in Ref. 1). When $\vec{H}$ is exactly along the c axis, the three electron sheets of the Fermi surface are degenerate, and the hole area is slightly lower. As $\vec{H}$ is rotated toward the binary axis, the three electron areas split, two changing rapidly in opposite directions and one remaining nearly constant. The hole area varies slowly, also (see Fig. 8). We have made extensive measurements in this region in an attempt to find both nonextremal areas and disappearance of signals. Both transmitted pulse height and its derivative with respect to magnetic field have been used.

No indication of nonextremal orbits was found in any of our measurements. The results of detailed measurements on sample II in this region are shown in Fig. 9. The solid dots are the dominant Fourier components of the signal, while the open circles are much weaker frequencies. The solid lines are extremal electron areas, and the heavy dashed line is the hole area. The short dashed lines are the predicted nonextremal areas. The large error bars at low angles are due to the

extreme weakening of the signal as $\vec{H}$ becomes normal to $\vec{q}$; no oscillations could be seen when $\vec{H}$ was exactly normal to $\vec{q}$. Only extremal areas can be seen, even when $\vec{H}$ is only 0.2° away from normal to $\vec{q}$.

While the relative settings of the sample holder orientation and magnetic field are reproducible to 0.2° or better, the absolute orientation of both $\vec{q}$ and $\vec{H}$ relative to the crystal axes can only be accurately determined from the data. The angle between $\vec{q}$ and $\vec{H}$ is known to 0.1° by means of the tilt effect. The relation of $\vec{H}$ to the crystal axes is then found by taking area data within about ± 10° of the major axis. Since the electron areas change very rapidly near the trigonal axis, the measured area can be compared to the theoretical ones and the absolute orientation of $\vec{H}$ found to within 0.2° in the binary-trigonal plane and 0.3° in the trigonal-bisectrix plane (the latter represents a tip of $\vec{H}$ out of the binary-trigonal plane). The theoretical areas were generated by a computer program that allowed $\vec{H}$ to be in any direction, and values for its orientation were tried until theory and experiment agreed. The only two adjustable parameters were the crystal miscut in the $\vec{q}$-$\vec{H}$ plane and the tip of $\vec{H}$ out of this plane. Thus, in Fig. 9, $\vec{H}$ is perpendicular to $\vec{q}$ at 0.4° from the c axis, indicating that $\vec{q}$ is 0.4° off of the binary axis owing to a miscut of the bismuth crystal. The three electron ellipsoids are not degenerate at 0° because H is tipped about 0.5° out of the binary-trigonal plane.

Examination of the data of Giura *et al.*[1] shows that they also saw only extremal oscillations. While they do not plot the areas for this orientation, the data in their Fig. 7 show the same period of oscillation on either side of the disappearance; there is no indication of the rapidly changing periods that would arise from nonextremal signals.

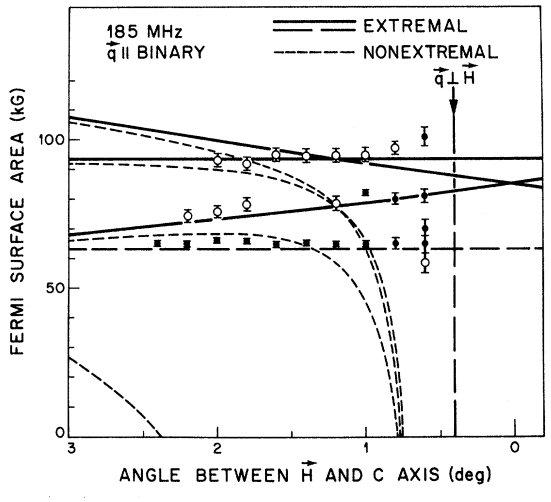

FIG. 9. Fermi-surface areas near $\vec{H} \perp \vec{q}$ in sample II. $\vec{q} \parallel$ binary axis and $\vec{H}$ is in the trigonal-binary plane.

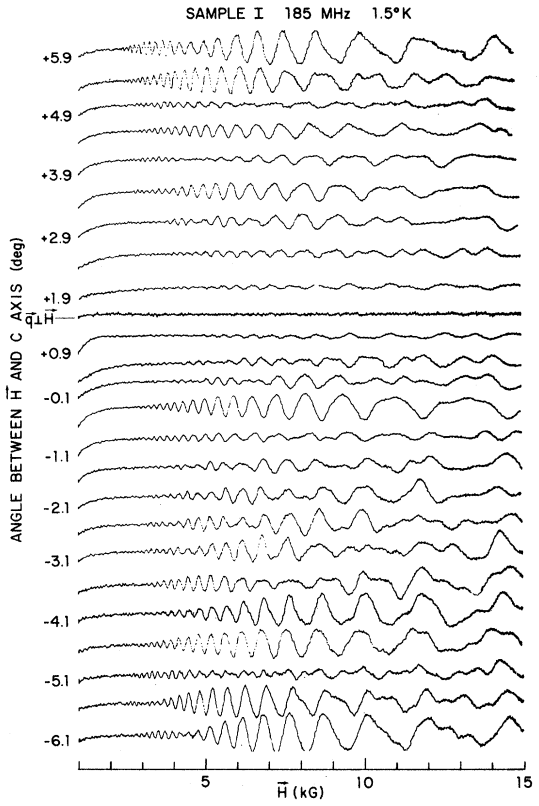

FIG. 10. Derivative of transmitted pulse height vs magnetic field for sample I with $\vec{q} \parallel$ binary axis and $\vec{H}$ in the trigonal-binary plane.

Although we have never seen the complete disappearance of signal for any orientation other than $\vec{H} \perp \vec{q}$, we have observed a weakening of the strength of the oscillations at certain angles. As an example, data taken in this region on sample I are shown in Fig. 10. Here the derivative of the pulse height is measured for various orientations of $\vec{H}$ and the c axis. (All traces were taken with the same gain settings.) The oscillations disappear completely only when $\vec{H} \perp \vec{q}$, as expected. A decrease in signal strength can be seen at +4.9°, +3.9°, −1.1°, and −5.1°, however. These are representative of the weakest we have seen the signal (except when $\vec{H} \perp \vec{q}$) in either sample. Attempts at changing all orientations of the crystal to further reduce the amplitude were unsuccessful.

To see the origin of these decreases, the Fermi surface areas determined from these data are plotted in Fig. 11. A crystal miscut of about 1.4° is present in this case, and $\vec{H}$ is tipped 0.8° out of the trigonal-binary plane, as determined from the splitting of the electron area degeneracy at 0°. Again, only extremal areas are seen, even

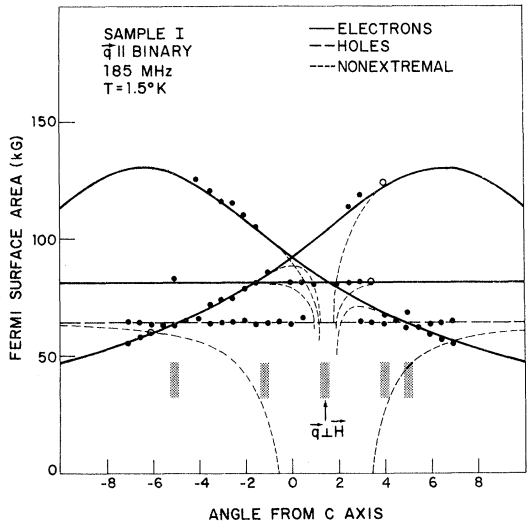

FIG. 11. Fermi-surface areas from data in Fig. 10.

within 0.5° of signal disappearance. The shaded areas indicate the angles where the signal strength decreased. They can all be seen to occur at places where two sheets of the Fermi surface have equal or nearly equal areas. They arise, of course, from the destructive interference of signals from the two sheets, as is borne out by the continuity of Fourier components through these regions.

The crossing of electron and hole areas is expected, of course, even if $\vec{H}$ is exactly in the trigonal-binary plane. The additional crossings of two electron sheets could easily be overlooked, however, if the misorientation of $\vec{H}$ were not considered. To see the effect of this tip, we made several runs with $\vec{H}$ purposely tilted out of the trigonal-binary plane; the results are shown in Fig. 12. The sample holder was nominally rotated in 1° intervals about the sound direction; the angles φ in Fig. 12 are the orientations of $\vec{H}$ used in the theoretical curves fit to these data. The degree of uncertainty in sample holder setting accounts for the deviation from 1° steps. Any substantial decrease in signal strength observed is represented by shading on the figure. Again all these regions are due to area crossings where the signals from each sheet have nearly equal amplitudes. It should be noted that a misorientation of $\vec{H}$ of 2° is sufficient to cause the two additonal crossings to be about 7° apart, as observed by Giura *et al.*

Since the amplitude of giant quantum oscillations from any sheet of the Fermi surface is proportional to the deformation potential coupling between the sound wave and the carriers on that sheet, as well as the carrier's effective mass,[2] the relative amplitude of oscillations from different sheets is strongly dependent on the orientation of $\vec{q}$ and the crystal

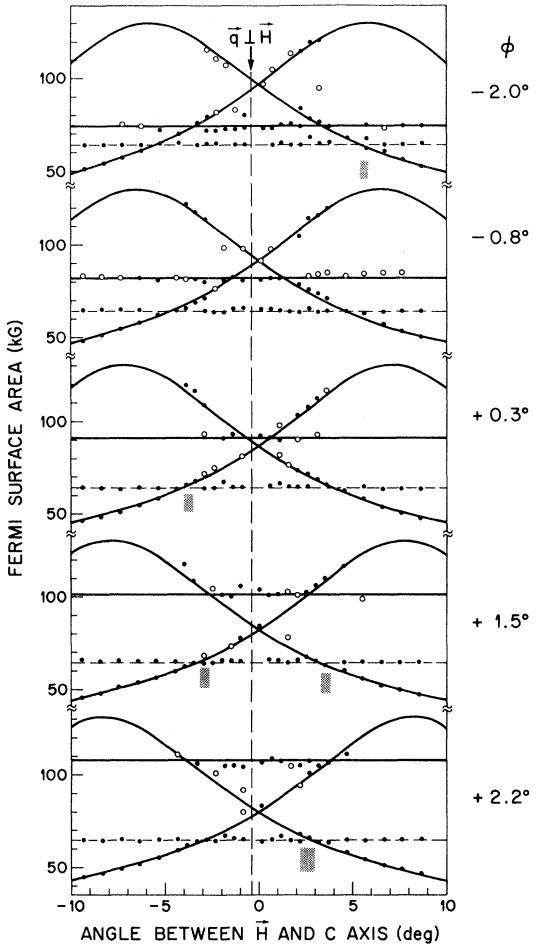

FIG. 12. Fermi-surface areas measured with $\vec{H}$ tipped by φ degrees from the trigonal-binary plane. Solid lines are theoretical extremal Fermi-surface areas for electrons and dashed lines are for holes. Shaded areas indicate regions of weak signal.

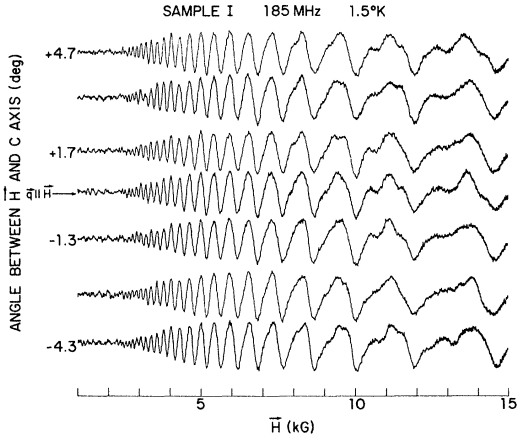

FIG. 13. Giant quantum oscillations for $\vec{q} \parallel$ trigonal axis and $\vec{H}$ in the trigonal-binary plane. Here $\vec{H}$ is nearly parallel to $\vec{q}$.

axes.[12,13] If $\vec{q}$ is along the trigonal axis and $\vec{H}$ is oriented as above, the hole sheet oscillation is much stronger than the electron oscillations, as shown in Fig. 13, and no appreciable weakening occurs even when electron and hole sheets cross. Since $\vec{q}$ is nearly parallel to $\vec{H}$ here, the signal never disappears, and all areas are exactly extremal. (This can be compared with Fig. 9 in Ref. 1.) Thus the lack of signal disappearance (or weakening, in our case) when $\vec{q}$ is along the trigonal axis in no way indicates that such effects are due to nonextremal areas when $\vec{q}$ is the binary direction, and thus nearly normal to $\vec{H}$.

From the above considerations, we suggest that the disappearance of oscillations seen by Giura *et al.*[1] in this orientation is probably due to destructive interference between signals from two electron sheets when $\vec{H}$ is tipped about 2° out of the trigonal-binary plane. The difference in size of signal reduction between our data and theirs could arise from different crystal miscuts and the associated deformation potential amplitude.

C. Bisectrix-Trigonal Plane

The other orientation in which Giura *et al.* saw the disappearance of oscillations was with $\vec{q}$ along the bisectrix axis and $\vec{H}$ about 6° from the trigonal axis in the trigonal-bisectrix plane (see Figs. 5 and 9 in Ref. 1). We have studied this region also, and the results of measurements on sample II are shown in Fig. 14. As before, the signal disappears when $\vec{H} \perp \vec{q}$, but there are no other angles where the signal gets very weak. In particular, nothing unusual happens in the neighborhood of +6°, not even the weakening seen in the binary-trigonal orientation. Comparing the areas measured here (Fig. 15) with Fig. 4 in Ref. 1 shows that it is indeed +6°, and not −6°, where the disappearance was seen. Tipping $\vec{H}$ out of the trigonal-bisectrix plane by several degrees does not introduce any new features in the data.

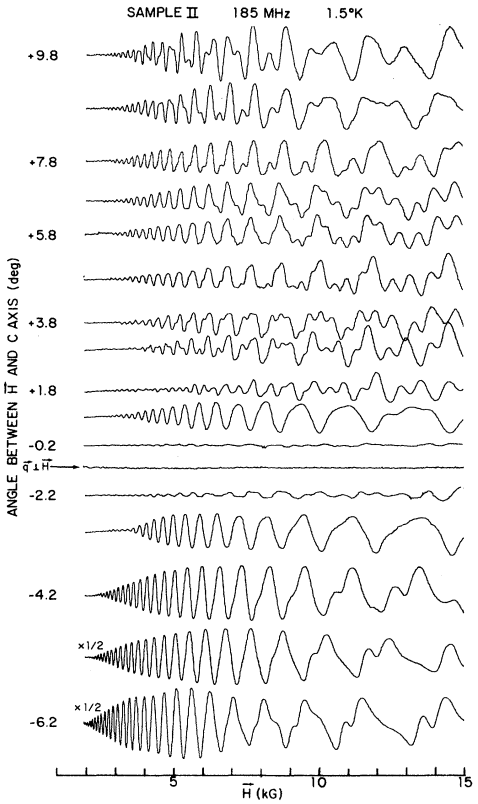

FIG. 14. Giant quantum oscillations in sample II for $\vec{q} \parallel$ bisectrix axis and $\vec{H}$ in the trigonal-bisectrix plane.

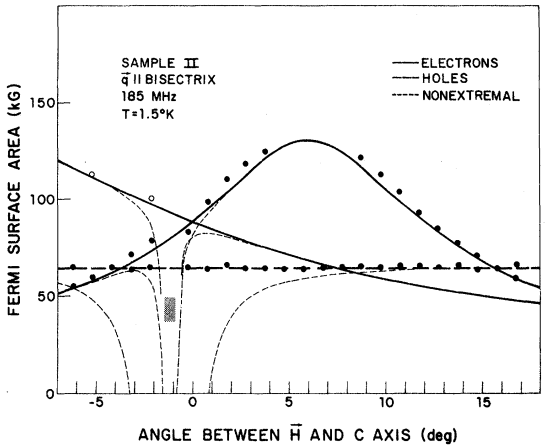

FIG. 15. Fermi-surface areas from data in Fig. 14.

The Fermi surface areas computed from these data are shown in Fig. 15. Here there is a 1.2° crystal miscut, so $\vec{q}$ is 1.2° away from the bisectrix axis. Again there is no indication of nonextremal areas, even within 0.5° of $\vec{H} \perp \vec{q}$. Giura *et al.* have plotted their measured areas in this orientation in Fig. 4 of Ref. 1. No nonextremal areas are present; the hole area has the extremal value on both sides of the disappearance at 6°, and, in fact, remains constant right up to the disappearance at $\vec{H} \perp \vec{q}$.

We do not have an explanation for the disparity between our results and those of Giura *et al.* in this orientation. There are two points that are worth noting, however. It has been observed previously that the deformation potential coupling between longitudinal acoustic waves propagating along the bisectrix axis and the two electron ellipsoids that transform into one another by reflection in the trigonal-bisectrix plane is either very weak or zero, and oscillations from them are not seen.[12,13] The only evidence we have for these two sheets in this orientation is two questionable points at −2.2° and −5.2° in Fig. 15. The angle

at which the area of these two sheets equals the hole area is within 1° of the disappearance reported by Giura *et al.* If $\vec{q}$ were far enough off the bisectrix axis (in any direction), these electrons would contribute to the signal, and beating effects might be observed. The magnitude of miscut necessary is difficult to estimate, however.

The second point is that at +6° the single electron sheet has a maximum area which is just twice that of the hole sheet, so that even harmonics of the hole oscillations have the same periods as those of the electrons. For our orientation of $\vec{q}$ relative to the bisectrix axis, the signal from the holes is larger than that from the electrons, and no appreciable loss of signal strength is observed. A different crystal miscut would change the relative strengths of these signals, however, and for some orientations the two signals might be close enough to the same size for some beating effects to occur. Again, the size of this effect is difficult to estimate.

VI. SUMMARY

In an attempt to verify the possible existence of a saddle point on the hole Fermi surface of bismuth, we have studied all sheets of the Fermi surface using giant quantum oscillations in the ultrasonic attenuation in very high quality single crystals. In previous experiments, Giura *et al.*[1] reported the disappearance of these oscillations for certain orientations and suggested that it might be caused by nonextremal Fermi-surface orbits tangent to a saddle point. We observe nonextremal orbits in only one orientation and in only one of our samples. They agree in both period and line shape with theory. In all other orientations, however, only the usual extremal areas are seen, and the disappearance of signal is not observed. Examination of the data of Giura *et al.* shows only extremal areas there, also. We thus find no evidence in support of a saddle point on any sheet of the Fermi surface. Some suggestions as to the possible origin of signal disappearance in terms of sample misorientation are made.

ACKNOWLEDGMENTS

The author would like to thank R. L. MacLean, A. J. Strauss, and R. A. Murphy for supplying the bismuth, J. G. Mavroides, F. A. Blum, and H. J. Zeiger for many helpful discussions, and B. Feldman for assistance in taking the data.

---

*Work sponsored by the Department of the U. S. Air Force.

[1]M. Giura, R. Marcon, T. Papa, and F. Wanderlingh, Phys. Rev. **179**, 645 (1969).

[2]V. L. Gurevich, V. G. Skobov, and Y. A. Firsov, Zh. Eksp. Teor. Fiz. **40**, 78 (1961) [Sov. Phys.-JETP **13**, 552 (1961)].

[3]H. N. Spector, Phys. Rev. **120**, 1261 (1960).

[4]M. S. Svirskii, Zh. Eksp. Teor. Fiz. **44**, 628 (1963) [Sov. Phys.-JETP **17**, 426 (1963)].

[5]V. E. Henrich, Phys. Rev. Lett. **26**, 891 (1971).

[6]For example, see A. N. Friedman and S. H. Koenig, IBM J. Res. Dev. **4**, 158 (1960).

[7]R. A. Murphy (private communication); R. Hartman, Phys. Rev. **181**, 1070 (1969).

[8]J. W. Cooley and J. W. Tukey, Math. Comput. **19**, 297 (1965).

[9]P. T. Panousis, Ph.D. thesis (Iowa State University, 1967) (unpublished).

[10]For a review of work through 1968, see Y. Shapira, in *Physical Acoustics*, edited by W. P. Mason (Academic, New York, 1968), Vol. V.

[11]T. Sakai, Y. Matsumoto, and S. Mase, J. Phys. Soc. Jap. **27**, 862 (1969).

[12]S. Inoue and M. Tzuji, J. Phys. Soc. Jap. **22**, 1191 (1967).

[13]K. Walther, Phys. Rev. **174**, 782 (1968).